Zeolite-Dye Microlasers

U. Vietze, O. Krauß, and F. Laeri*
Darmstadt University of Technology, D-64289 Darmstadt, Germany

G. Ihlein and F. Schüth
University of Frankfurt, D-60439 Frankfurt, Germany

B. Limburg and M. Abraham
IMM, D-55129 Mainz, Germany
(Received 26 March 1998)

We present a new class of micro lasers based on nanoporous molecular sieve host-guest systems. Organic dye guest molecules of 1-ethyl-4-[4-(*p*-dimethylaminophenyl)-1,3-butadienyl]-pyridinium Perchlorat were inserted into the 0.73-nm-wide channel pores of a zeolite $AlPO_4$-5 host. The zeolitic microcrystal compounds were hydrothermally synthesized according to a particular host-guest chemical process. The dye molecules are found not only to be aligned along the host channel axis, but to be oriented as well. Single mode laser emission at 687 nm was obtained from a whispering gallery mode oscillating in a 8-μm-diameter monolithic microresonator, in which the field is confined by total internal reflection at the natural hexagonal boundaries inside the zeolitic microcrystals. [S0031-9007(98)07791-6]

PACS numbers: 42.55.Mv, 42.60.Da, 61.43.Gt, 61.66.Fn

Structures of optical wavelength scale such as microresonators and microlasers are presently attracting considerable attention in quantum optics, laser physics, materials science, and device technology. The reduction of at least one lateral dimension of a laser structure down to the order of one wavelength modifies the mode density of the optical field inside the laser resonator which in turns modifies the spontaneous emission rate [1]. As a result, the light generation efficiency in wavelength-scale microlasers is expected to increase. In addition, the cavity quantum electrodynamic effects that are predicted to appear in this regime can be exploited to accomplish novel functions [2,3].

From an experimental point of view, reducing the size of a laser necessitates that careful attention be given to the scaling laws of the two basic parameters gain and losses. On one hand, the gain of the light propagating in the laser structure scales in general with the propagation length, as do the scattering losses in the medium. On the other hand, the coupling losses from the inside to the outside of the laser structure do not depend on geometrical factors. Consequently, even for laser media with very low scattering losses, scaling down to the size of a few wavelengths becomes difficult because the reduced gain can no longer compensate for the coupling losses. Up to now, laser size reduction down to a few ten micrometers has been sucessfully carried out for media with high gain, such as semiconductors (vertical cavity surface emitting lasers, microdisk [2,4], or spherical lasers [5]), and sperical liquid [6], or polymer dissolved dyes [7,8], as well as solid state spheres [9]. Thus, realizing wavelength scale lasers based on alternative materials, geometries, and emission wavelengths is still a challenging experimental task. As a reward, in addition to a gain in their basic understanding, one can imagine many practical applications for microlasers, e.g., as efficient luminophores, or as bright lasing pixels for displays [10].

In this Letter, we report the first realization of a new class of solid sate microlasers based on a host-guest composite material. In contrast to conventional gain materials, in which the active centers are not systematically ordered on the microscopic level, the regular crystallographic matrix of cavities in a zeolite crystal maintains the laser active organic guest molecules aligned and oriented. In fact, the aluminosilicate structure of zeolitic crystals surrounds regularly arranged cavities or channels with a size of up to about 1×10^{-9} m [11,12]. It is this framework of crystallographically arranged nanometer cavities that has stimulated physicists, chemists, and materials scientists to investigate guest-host modifications of the host material on the nanometer scale, with the objective of tailoring the properties of the composite on the macroscopic scale. For example, Bogomolov *et al.* [13] synthesized nanocomposites of semiconductor-based clusters in zeolites and superconducting quantum wires [14], whereas Cox *et al.* [15] presented a concept for the modification of the nonlinear optical response of molecular sieve materials. Further applications based on the inclusion concept were proposed, cf., e.g., Refs. [16–18]. For optical functions, the inclusion ansatz was first successively embodied by Cox *et al.* [19]. The group of Caro and Marlow [20] also transformed various AlPO and SAPO molecular sieves into a nonlinear material for optical frequency conversion by inclusion of the noncentrosymmetric organic molecule *p*-nitroaniline, and Bredol *et al.* [21] included efficient luminophores in zeolites.

 0031-9007/98/81(21)/4628(4)$15.00

The framework of the hexagonal ($P\frac{6}{m}cc$) $AlPO_4$-5 crystals discussed here consists of a one-dimensional system of pores (channels) 0.73 nm wide. Guided mainly by geometrical considerations, we selected the dye molecule 1-ethyl-4-[4-(*p*-dimethylaminophenyl)-1,3-butadienyl]-pyridinium Perchlorat (Pyridine 2) [22] as a luminescent activator center. With a width of about 0.6 nm (calculated with the code SHELXTL) it fits into the one-dimensional channel framework of the zeolite $AlPO_4$-5 [23]; cf. Fig. 1. The dye molecules were brought into the pores by *in situ* inclusion of the organic dyes during the synthesis [24], a method pioneered by the group of Schulz-Ekloff and Wöhrle [25]. The compound was hydrothermally synthesized as described in Ref. [26]. An ice cold solution of triethylamine, phosphoric acid, Pyridine 2, and water was added under stirring over 10 min to an aluminumoxidehydroxide suspension prepared as described in Ref. [27]. The mixture was stirred for another 20 min, and filled into a Teflon lined autoclave, which then was placed in an oven preheated to 210 °C. Usually, after short reaction times of about 1 h, one obtains mostly regularly shaped hexagonal prisms, whereas longer reaction times lead preferentially to dumbbell-shaped crystals where the prismatic center bar splits off into a fasciclelike ensemble of diverging prismatic needles; cf. Fig. 3(b) below. These crystals are characterized by the regular shape of their prismatic central part, which with a width of about 8 μm, can act as a laser resonator [Fig. 3(c) below]. The color distribution observed in the light microscope indicates that the dye concentrates in this central part, whereas the fascicled end parts appear colorless, implying a low dye content. Consequently, laser action was observed in the prismatic central region of the dumbbell-shaped crystals. Whatever the crystal shape, x-ray powder diffractograms reveal no indication of the presence of any crystallographic phase other than ($P\frac{6}{m}cc$)$-AlPO_4$-5. After the desired reaction time, the autoclaves are quench cooled, the crystals filtered out, rinsed with water, and dried. Their refluxing in ethanol did not reveal any extraction of dye inclusions. Syntheses with dye concentrations between 0.1% mass and 0.01% mass were realized.

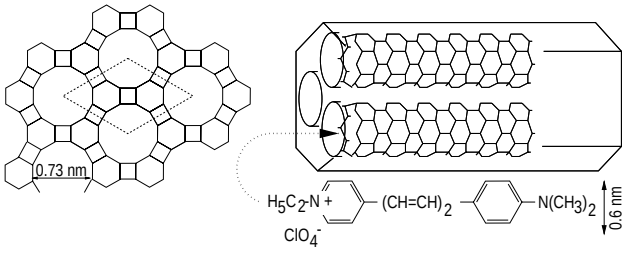

FIG. 1. The zeolite $AlPO_4$-5, its one-dimensional channel framework, and the inserted dye molecule 1-ethyl-4-[4-(*p*-Dimethylaminophenyl)-1,3-butadienyl]-pyridinium Perchlorat (Pyridine 2).

The long axis of the Pyridine 2 dye guest molecules line up along the channel pores of the $AlPO_4$-5 host, resulting in a composite with strong macroscopic dichroic properties. The crystal appears dark red or transparent, depending on the direction of the polarization vector of the incident light with respect to the channel direction. Furthermore, the Pyridine 2 molecule is an electron pushpull system carrying an electric dipole moment along its axis. *A priori*, inclusion into the channel pores can occur with the dipole moments all aligned in parallel, or with alternating antiparallel orientation. In the first case the dipole moments add to a static macroscopic moment, whereas in the latter case the net macroscopic moment vanishes. Our investigations of single crystal individuums revealed that, with the inclusion of Pyridine 2 dyes, the AlPO crystals acquire pyroelectrical properties, implying the presence of a macroscopic moment. Thus, in contrast to the random orientation of the dye molecules in liquid or polymeric laser media, the dye molecules in the zeolite solid state system are not only aligned but, on average, are oriented as well.

The samples are optically pumped with the second harmonic of a Q-switch Nd:YAG laser ($\lambda = 532$ nm, 10 ns pulse length, 10 Hz repitition rate). The excited fluorescence light was collected with a microscope objective (numerical aperture $NA = 0.35$). Behind the sample the pump light was warded off with a 3 mm Schott RG 610 filter. The imaging magnification of the sample on the CCD chip of the cooled imaging camera (Photometrics CH250 running at -20 °C) was 55×. In order to increase the light collection efficiency without perturbing the imaging properties of the spectrometer (ORIEL MS 257 with 600 lines/mm, 400 nm blaze wavelength grating, and InstaSpec IV detector, slit width about 150 μm), the magnification perpendicular to the entrance slit was, when needed, reduced to about 5× with a cylindrical lens. The imaging camera and the spectrometer were carefully aligned to collect and display the fluorescence signals originating from the very same sample area. At the same time, the data acquisition time window of the spectrometer was synchronized with the camera acquisition cycle. In summary, we made certain that the captured spectra could be uniquely associated in space as well as in time with the images acquired by the camera. With this technique we analyzed samples in a heap, as well as isolated single individual crystals.

To prevent intersystem crossing processes (energy transfer to nonluminescent, long living triplet states) from quenching the fluorescence, the system is pumped with 10 ns pulses. The oriented inclusion of the dye molecules results in a strongly polarized fluorescence emission. The fluorescence distribution of the microcrystal individuals investigated peaks at about 685 nm and exhibits a FWHM of about 85 nm. When the pulse energy used to pump a number of clumped microcrystals (>100) is increased above a certain threshold, we observe the sudden appearance of strong spectral spikes around the fluorescence maximum. The spikes exhibit an instrument

limited width of about 0.6 nm and a spacing of about 4 nm. With increasing pump energy, the spikes grow at a faster rate than the fluorescence shoulder, as illustrated in Fig. 2. The presence of a threshold energy together with the rapid intensity increase with pump power are signatures of the stimulated emission processes occurring in a laser. Note that in Fig. 2 the contribution of the collected fluorescence light originates from a heap of microcrystals imaged to fill the entrance slit area, whereas the contributions to the spectral peaks originate in small localized spots, as will be shown below. Thus, the peak-to-shoulder ratio corresponding to a single localized laser emitter is grossly underestimated in Fig. 2.

Inspection of individual crystals revealed that only samples with a dumbbell-like shape show laser emission, most of them oscillating on several spectral lines. However, a number of specific individuals were found to emit a single line. A typical example is shown in Fig. 3 with its emission spectrum (a) and the corresponding SEM (b) and optical (d) micrographs. As seen in Fig. 3(d), the strong part of the fluorescence activity is concentrated in the prismatic central section of the dumbbell sample within a 3–4-μm-wide slice. This is compatible with the distribution of the dye concentration visible as red coloration when inspecting the sample with the light microscope. As a consequence, this strong concentration of dyes, and thus gain, in a thin slice can confine the oscillating field through gain guiding. Superimposed to the below threshold luminescence image are the localized spots, from where the strong laser lines were emitted. Figure 3(e) shows the spectral distribution of the emission as a function of the image height. We see that the strong, narrow line emission emerges from a position which is consistent with the spots of strong emission shown in the micrograph [Fig. 3(d)]. As already mentioned, the luminescence is linearly polarized parallel to the crystal axis because of the orientation of the molecular polarizability of the included dye molecules. For this reason, luminescence emission, and thus also any stimulated emission, in the direction of the crystal axis is not possible. Therefore, light amplification can only occur for waves traveling in planes normal to the crystal axis. In fact, there exists a wide range of wave vectors parallel to the high gain slice, which fulfill the conditions for total internal reflection (TIR) at the prism faces. The faces of the prism therefore form the mirrors of an optical ring resonator in which the necessary feedback for laser action is provided; cf. Fig. 3(c). The optical mode oscillating in this ring resonator resembles a whispering gallery mode. Whispering gallery modes were extensively discussed [2,3,28], and, as mentioned at the beginning, lasing was observed in different geometries. In our case the mode is confined by the prism faces and by gain guiding in a 3–4-μm-thick disk. We estimate the gain-induced index increase to be about 10^{-3}, sufficient to confine the field [29]. Together with the narrow width of the gain region, this leads to single frequency oscillation. In fact, in samples in which the dye was contained in wider disks, multiline emission was observed. The lasing threshold for single microlasers was approximately 12×10^{-9} J pump energy falling upon the about 200-(μm)^3 volume enclosing the lasing mode (dye concentration about 0.05% mass). In an ideal whispering gallery mode only minuscule amounts of diffracted light will leave the resonator [30]. In the sample shown, laser light is outcoupled at small defects at the crystal surface which disturb the TIR; cf. the hot spots in Fig. 3(d). The roundtrip length for the light circulating in this ring resonator is about $\ell \approx 25$ μm, corresponding to a longitudinal mode separation $\Delta\lambda = \lambda^2/n\ell$ of about 13 nm. This is more than 3 times the spectral line spacing observed in crystals exhibiting multispike emission. We suspect that these lines correspond to different morphology-dependent structure modes, analoguous to those observed in spherical lasers [6].

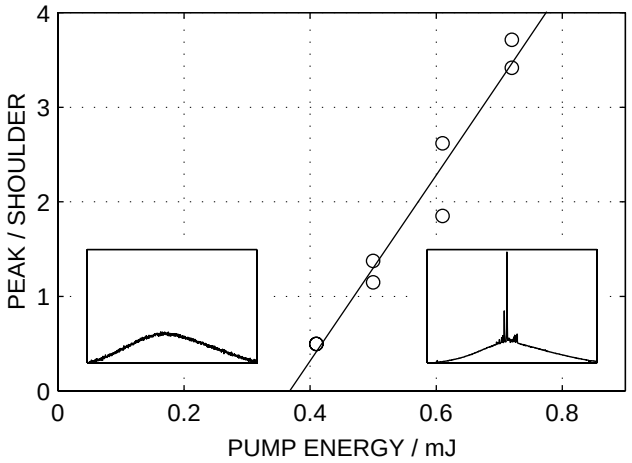

FIG. 2. Ratio of the height of a spectral peak above the shoulder to the fluorescence shoulder height as a function of the energy of the unfocused laser pulses ($D_{\text{laser}} = 1.2$ mm) pumping an ensemble of crystal samples. The diagram reveals the presence of a threshold and an overproportional growth for the spectral spike intensity. Shown in the insets are typical spectra below and above threshold (not scaled). Note that, as the laser emission (spectral spikes) is strongly directed, not all of the emitted laser light from the samples is collected by the spectrometer aperture.

Although we did not systematically investigate size-dependent effects yet, we have demonstrated laser emission in composite material microlasers with a resonator size in the regime where size-dependent effects such as reduction of laser threshold [1,31] start to play a role. To our knowledge, the microlasers presented here are about 3× smaller than the smallest dye lasers realized so far [7]. In addition, the dye molecules are uniformly aligned in the zeolitic solid state host. In this system, we also observed fluorescence emission (yet not laser emission) excited by the two photon absorption of 1064 nm laser light as well as frequency conversion of the 1064 nm excitation to its 532 nm second harmonic.

This work was funded by the Deutsche Forschungsgemeinschaft DFG.

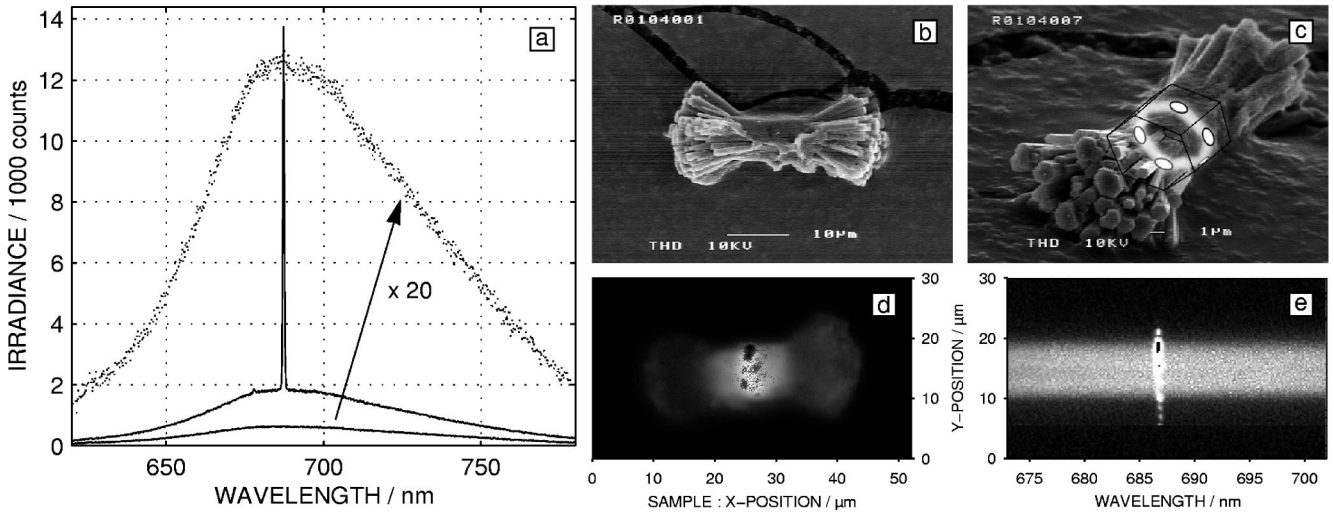

FIG. 3. (a) Emission spectra of the dumbbell-shaped $AlPO_4$-5−Pyridine2 compound microcrystal individual are shown in this figure below lasing threshold and above threshold. (b) Scanning electron microscope (SEM) image of the AlPO sample discussed here. (c) SEM image of a microcrystal, outlining the hexagonal middle section forming the optical resonator providing the feedback by total internal reflection (whispering gallery mode). (d) Optical micrograph of the spacial distribution of the luminescence emission taken at the same time as the subthreshold spectrum shown in (a). Superimposed on the subthreshold luminescence distribution, and digitally coded in black with conventional image processing tools, are those spots where the laser spike apparent in (a) is emitted. (e) On the spectrometer input the horizontal image magnification is reduced with an anamorphoticlike imaging system so that the whole crystal length can pass through the entrance slit. The imaging properties of the spectrometer allow one to spatially resolve the light distribution along the entrance slit. The figure shows the spectrum along the entrance slit (scale matched to the figure at left), where the irradiance is rendered in grey levels. The strong laser emission peak at 687 nm exceeds the dynamic range spanned by the grey scale and is therefore coded with black pixels. It is clearly shown that the laser emission emerges from regions corresponding to the black coded spots in (d).

*Author to whom all correspondence should be addressed. Institute of Applied Physics, Darmstadt University of Technology, D-64289 Darmstadt, Germany.
Email address: franco.laeri@physik-tu-darmsstadt.de

[1] H. Yokoyama *et al.,* in *Confined Electrons and Photons: New Physics and Applications,* edited by E. Burstein and C. Weisbuch (Plenum, New York, 1995); G. Bjork *et al., ibid.*
[2] *Microcavities and Photonic Bandgaps: Physics and Applications,* edited by J. Rarity and C. Weisbuch (Kluwer, Dordrecht, 1996); *Advances in Atomic Molecular and Optical Physics,* edited by P. Berman(Academic, New York, 1994), Suppl. 2.
[3] *Quantum Optics of Confined Systems,* edited by M. Ducloy and D. Bloch (Kluwer, Dordrecht, 1996).
[4] C. Gmachl *et al.,* Science **280**, 1556 (1998).
[5] M. Nagai *et al.,* Opt. Lett. **22**, 1630 (1997).
[6] H. M. Tzeng *et al.,* Opt. Lett. **9**, 499 (1984).
[7] M. Kuwata-Gonokami *et al.,* Jpn. J. Appl. Phys. 2, Lett. **31**, L99 (1992); K. Kamada et al., Chem. Phys. Lett. **210**, 89 (1993).
[8] R. K. Chang *et al.,* in *Quantum Optics of Confined Systems* (Ref. [3]), p. 75 .
[9] V. Sandoghdar et al., Phys. Rev. A **54**, R1777 (1996).
[10] N. Lawandy, *et al.,* Laser Focus **33(5)**, 137 (1997).
[11] J. V. Smith, Chem. Rev. **88**, 149 (1988).
[12] T. Zoltai, Am. Mineral. **45**, 960 (1960).
[13] V. N. Bogomolov *et al.,* Pis'ma Zh. Eksp. Teor. Fiz. **23**, 528 (1976).
[14] V. N. Bogomolov, Fiz. Tverd. Tela (Leningrad) **15**, 1312 (1973).
[15] S. D. Cox *et al.,* J. Am. Chem. Soc. **110**, 2986 (1988).
[16] N. Herron *et al.,* J. Am. Chem. Soc. **111**, 530 (1989).
[17] G. A. Ozin *et al.,* Angew. Chem., Adv. Mater. **101**, 373 (1989).
[18] G. D. Stucky and J. E. Mac Dougall, Science **247**, 669 (1990).
[19] S. D. Cox *et al.,* Chem. Mater. **2**, 609 (1990).
[20] F. Marlow and J. Caro, Zeolites **12**, 433 (1992).
[21] M. Bredol *et al.,* Adv. Mater. **3**, 361 (1991).
[22] Pyridine 2 is a trade name; cf. U. Brackmann, *Lambdachrome Laser Dyes,* (Lambda Physik, Göttingen, 1994), 2nd ed., pp. 198–199.
[23] W. M. Meier and D. H. Olson, *Atlas of Zeolite Structure Types* (Butterworth, Oxford, 1987), 2nd ed., pp. 18–19.
[24] G. Ihlein *et al.,* Appl. Organomet. Chem. **12**, 305 (1998).
[25] S. Wohlrab *et al.,* Zeolites **12**, 862 (1992); A. Sobbi *et al.,* Zeolites **15**, 540 (1995).
[26] D. Demuth *et al.,* Microporous Mater. **3**, 473 (1995).
[27] S. A. Schunk *et al.,* Microporous Mater. **6**, 273 (1996).
[28] V. B. Braginsky *et al.,* Phys. Lett. A **137**, 393 (1989); L. Collot *et al.,* Europhys. Lett. **23**, 327 (1993).
[29] O. Hess and T. Kuhn, Prog. Quantum Electron. **20**, 84 (1996).
[30] B. R. Johnson, J. Opt. Soc. Am. A **10**, 343 (1992).
[31] F. De Martini and G. R. Jacobovitz, Phys. Rev. Lett. **60**, 1711 (1988).